

## Size Effects in Flow of Flux-Line Solids and Liquids

M. H. Theunissen,<sup>1</sup> E. Van der Drift,<sup>2</sup> and P. H. Kes<sup>1</sup>

<sup>1</sup>*Kamerlingh Onnes Laboratory, Leiden University, 2300 RA Leiden, The Netherlands*

<sup>2</sup>*Delft Institute of Microelectronics and Submicron-technology, Delft University of Technology, 2600 GA Delft, The Netherlands*  
(Received 1 March 1996)

Flow of 2D flux lines confined to narrow channels has been studied. In the solid, (in)commensurability between lattice and channel width cause mobility oscillations from which the actual channel width follows. In the liquid, the oscillations disappear and flow is dictated by the shear viscosity  $\eta$ . By repeated experiments for different channel widths,  $\eta$  is determined for the first time. It diverges according to  $\eta \propto \xi_+^2(T, B)$ . An indication for the hexatic-to-liquid transition is also observed. [S0031-9007(96)00579-0]

PACS numbers: 74.60.Ge

The appearance of a flux liquid just below the upper critical field  $B_{c2}$  has been predicted to be a general property of the mixed state [1]. This prediction was largely ignored until recently Nelson suggested that the absence of zero resistance in a magnetic field observed in high temperature superconductors is caused by a transition to the flux liquid state [2]. At present, a variety of experiments provided evidence for melting (even in presence of weak disorder), both for a three dimensional (3D) vortex lattice [3] and for a 2D vortex lattice [4].

Now that the existence of a flux liquid is well established, one may focus on its properties, particularly, the appearance of a dynamic shear viscosity  $\eta(T, B)$  in place of a shear modulus  $c_{66}$ . The shear modulus should discontinuously disappear at melting when the shear fields vary slowly in both space and time [5]. The behavior of  $\eta$  close to freezing is especially interesting, since the (hexatic) liquid then may be considered as a solid with a low density of free dislocations (i.e., dislocation loops in 3D [6] and edge dislocations in 2D [7]). Concentrating on the 2D case being the actual situation in our experiments, we follow Nelson's suggestion [8] that  $\eta$  is inversely proportional to the density of free dislocations  $n_f$  which itself is determined by the translational correlation length  $\xi_+$  in the liquid given by

$$\eta(T, B) \sim 1/a_0^2 \bar{\mu} n_f \sim \xi_+^2(T, B), \quad (1)$$

with  $a_0$  the lattice spacing and  $\bar{\mu}$  a typical dislocation mobility. Approaching the melting line  $T_m(B)$  from above,  $\eta$  mimics the strong divergence of  $\xi_+$ , i.e.,

$$\begin{aligned} \xi_+ &= \xi_{+0} \exp \left[ b' \left( \frac{T_m}{T - T_m} \right)^\nu \right] \\ &= \xi_{+0} \exp \left[ b'' \left( \frac{B_m}{B - B_m} \right)^\nu \right], \end{aligned} \quad (2)$$

with  $\nu = 0.36963\dots$ ,  $b'$  and  $b''$  nonuniversal constants of order unity, and  $\xi_{+0} \approx a_0$  being the smallest length scale of the system.

In order to probe this behavior we extended the experiment of Pruijboom *et al.* [9] who studied the flow

of a vortex solid through narrow channels in a double layer device. We designed similar devices consisting of an amorphous  $\text{Nb}_3\text{Ge}$  bottom layer (thickness 500 nm) covered with a 50 nm thick NbN layer. Using nanolithography 300 identical, parallel channels were etched through the NbN layer into the NbGe, one channel in each 10  $\mu\text{m}$ , down to a depth of 240 nm from the top surface leaving a layer of 310 nm  $a\text{-Nb}_3\text{Ge}$ ; see Fig. 2(b) inset. Different samples with channel widths ranging between  $238 < w < 1185$  nm were made in a four-point terminal configuration with the voltage probes next to the channel array and the current flowing perpendicular to the channels. The width of the samples was 300  $\mu\text{m}$ . In a perpendicular magnetic field the flux lines experience a Lorentz force in the direction of the channels. In the solid, the flux lines outside the channels are pinned in

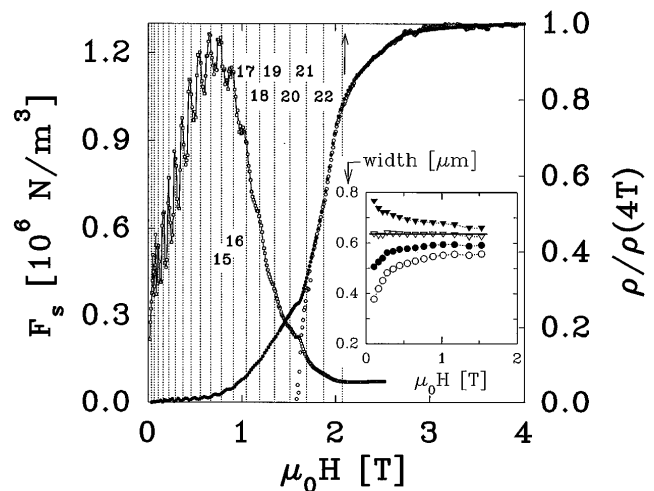


FIG. 1. Shear force  $F_s$  ( $\square$ ) and  $\rho_{ac}$  ( $\circ$ ) and  $\rho_{dc}$  ( $\bullet$ ) as a function of field at  $T = 1.70$  K for the sample with  $w = 637$  nm. Dashed lines are predictions for peak fields according to Eq. (5). The transition from Ohmic to non-Ohmic behavior coincides with the “unexpected” peak between  $N = 20$  and 21. The arrow denotes  $B_{c2}$ . The inset shows the channel width computed from the peak fields according to Eq. (5). From top to bottom results for  $N_0 = 8, 7, 6, 5$ . For  $N_0 = 7$  a horizontal line is obtained at  $w = 637$  nm.

the strong pinning NbN layer (with  $j_c$  in NbN  $\geq 10^4 j_c$  in NbGe), while those inside the channels will start to move as soon as the Lorentz force surpasses the shear interaction with the pinned vortices at the channel edges. The condition for plastic shear flow in the continuum approximation can be written as  $F_s = j_s B = 2\tau/w$ , where  $\tau = Ac_{66}$  is the flow stress. The parameter  $A$  depends on the flux line lattice configuration inside the channels, e.g., when the lattice parameter is commensurate to the channel width  $A \approx 0.05$ , but at incommensurability misfit dislocations will develop along the edges which reduces  $A$ . Measured as a function of field,  $F_s$  thus globally follows  $c_{66} \propto b(1-b)^2$ , with  $b = B/B_{c2}$ , but also oscillates with changing commensurability being maximum for perfect matching; see Fig. 1. In Ref. [9], two periodicities were observed at small flow velocities corresponding to two lattice orientations with respect to the channels. It turns out that at higher velocities the orientation with closed packed direction parallel to the channel is the stable one. Here we present only results for this orientation taken at a voltage criterion of 0.1 V/m per channel ( $v > 0.05$  m/s).

In the liquid phase,  $c_{66} = 0$  and the oscillations in  $F_s(B)$  should disappear. The flow through the channels (defined by  $y = \pm w/2$ ) is now controlled by the Bardeen-Stephen drag parameter  $\gamma$  [10] and the shear viscosity  $\eta$ . The velocity profile follows from the (simplified) hydrodynamic equation [11]

$$-\gamma \vec{v} + \eta \nabla_{\perp}^2 \vec{v} + \vec{f}_T = 0 \quad (3)$$

and the boundary condition  $\vec{v}(\pm w/2) = 0$ . The driving force  $\vec{f}_T$  is in the  $x$  direction. The velocity profile is maximum at  $y = 0$  and decays exponentially at the edges in a length scale  $\delta = \sqrt{\eta/\gamma}$ . The integrated velocity determines the net flow through the channel and the flux flow resistivity  $\rho_f$  to be measured:

$$\rho_f = \rho_f^0 [1 - (2\delta/w) \tanh(w/2\delta)], \quad (4)$$

where  $\rho_f^0 = B^2/\gamma$  is the Bardeen-Stephen value in which small corrections for weak pinning are supposed to be absorbed. This means that  $\rho_f^0$  should be measured independently. We therefore prepared a reference sample which has only one "channel" of  $w = 3$  nm.

The double layers are fabricated by RF-sputter deposition [9]. Pattern transfer into the NbN layer is performed by reactive ion etching in a mixed SiCl<sub>4</sub>-Cl<sub>2</sub>-He plasma [12]. The width and depth of the channels were determined by atomic force microscopy (AFM) and alpha step. We carried out a series of four-probe  $I$ - $V$  measurements on all samples, both in a dc and an ac (120 Hz) mode, as a function of field at  $T = 1.70, 2.00, 2.20,$  and  $2.40$  K and as a function of temperature at  $B = 1.00, 0.70, 0.50,$  and  $0.30$  T. Characteristic parameters of our two layer devices are  $T_c = 11.4$  K and  $B_{c2}(0) \approx 16$  T for the NbN top layer, and  $T_c = 2.68$  K,  $\Delta T_c = 10$  mK, and  $B_{c2}(0) = 3.8$  T [5], residual resistivity  $\rho_0 = 2.17 \mu\Omega$  m and  $dB_{c2}/dT|_{T_c} =$

$-2.1$  T/K for the NbGe reference sample. The upper critical field was originally determined by linear extrapolation of  $\rho_{ac}(T, B)$  to the normal state resistivity  $\rho_n$  [4]. The superconducting parameters determined from these data are  $\xi(0) = 7.7$  nm,  $\lambda(0) = 0.94 \mu$ m,  $\kappa = 75$ , and  $B_c(0) = 30.0$  mT.

A typical result of a  $F_s$  versus  $B$  plot is shown in Fig. 1 for the sample with  $w = 631 \pm 10$  nm (AFM) measured at  $T = 1.70$  K for decreasing field. For increasing field the peaks occur at the same field denoting one preferential lattice orientation for sufficiently large velocities. A substantial contribution to  $F_s$  ( $\geq 10^5$  N/m<sup>3</sup>) is related to the flux flow ( $B < B_{c2}$ ) or the normal state resistivity ( $B > B_{c2}$ ). Obviously  $F_s$  should be zero in the latter case. We now focus on the values of the peak field  $B_{\max}$  from which the effective channel width  $w_{\text{eff}}$  for vortex flow is determined. This parameter is essential for the interpretation of the data. We assume that  $w_{\text{eff}}$  is the distance between the first rows of strongly pinned vortices in the NbN layer near the channel edges, i.e.,  $w_{\text{eff}} = w + 2x_1 - b_0$ , where  $x_1$  is the distance of the first row to the channel edge and  $b_0 = a_0\sqrt{3}/2$ . Since the depth of the channel from the top is 40% of the total length of the vortex, we take for  $x_1$  the equilibrium value [13]:  $x_1 = (b_0/2)[1 + f_e(B/B_{c2})]$ , where  $f_e(B/B_{c2})$  expresses the contribution due to screening currents at the surface. In the field range of interest  $f_e \approx 0.607 - 1.05$ . Using an interpolation formula given in [14],  $x_1$  can be computed at any field. As noted above, the vortex lattice at  $B_{\max}$  is commensurate with the effective channel width, which gives

$$w_{\text{eff}} = w + 2x_1(B_{\max}) - b_0 = (N - 1)b_0(B_{\max}), \quad (5)$$

with integer  $N \geq 3$ . In order to find both  $N$  and  $w$  we computed  $w$  from Eq. (5) for different  $N_0$  in  $N = N_0 + n$ , where  $n = 0, 1, 2, 3, \dots$  numbers the maxima. For the correct  $N_0$  this procedure should give a horizontal line in a plot of  $w$  versus  $B_{\max}$ , as illustrated in the inset of Fig. 1. We thus obtain  $N_0 = 7$  and  $w = 637 \pm 3$  nm. The resulting values of  $N$  are given in Fig. 1. This means that the first row of weakly pinned vortices is located at the channel edge similar to the scenario where vortices are trapped by a step in the penetration depth (or thickness) [15]. The values of  $w$  obtained from the analysis are in good agreement with the values obtained from the AFM.

We denote in Fig. 1 the expected positions of the peaks by means of dotted lines. It shows that there is an unidentified peak at  $B \approx 1.6$  T and no further peaks at  $N = 21$  and  $22$ . The origin of the extra peak is clarified by adding in Fig. 1 plots of the dc resistivity ( $j_{\text{dc}} = 1.1 \times 10^6$  A/m<sup>2</sup>) and ac resistivity ( $j_{\text{dc}} = 0$  and  $j_{\text{ac}} = 2.8 \times 10^3$  A/m<sup>2</sup>). A dip in  $\rho_{\text{dc}}$  is seen at the position of the extra peak at 1.6 T. Just below this field  $\rho_{\text{ac}}$  begins to increase steeply and merges with  $\rho_{\text{dc}}$  at a field which lies slightly above the dip in  $\rho_{\text{dc}}$ . The transition from Ohmic to non-Ohmic behavior is known to be the best indication for the melting transition [3,4] in

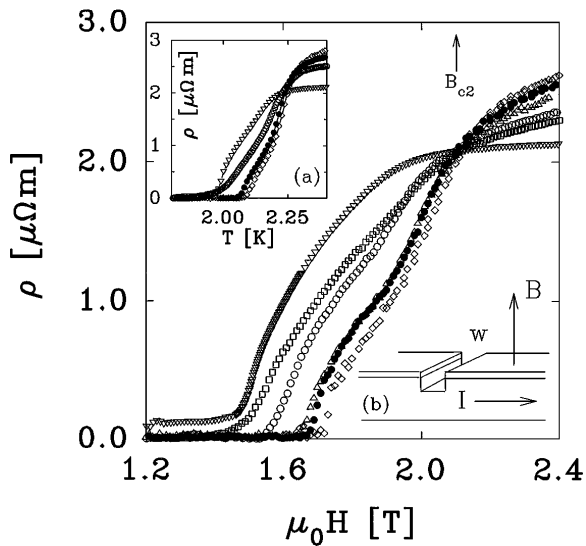


FIG. 2. Size effect of the vortex lattice melting as shown by  $\rho_{ac}(B)$  data at  $T = 1.70$  K for several channel widths: the reference sample ( $\nabla$ ),  $w = 1195$  nm ( $\square$ ), 637 nm ( $\circ$ ), 373 nm ( $\triangle$ ), 306 nm ( $\bullet$ ), and 245 nm ( $\diamond$ ). Inset (a) shows  $\rho_{ac}(T)$  results at 1.00 T, same symbols. Inset (b) displays a schematic view of a single channel.

a weakly disordered vortex lattice. We interpret the dip in  $\rho_{dc}$  as an indication that just before melting the shear modulus decreases due to plasticity [4,16], but remains finite in congruence with the dynamic picture of melting at finite wavelengths related to weak disorder [8]. We conclude that at about 1.6 T we observe a distinct, but gradual transition from a vortex solid to a liquid.

Up to  $B_{c2}$  we probe the liquid phase which explains the absence of peaks in  $F_s$ . A kink in  $\rho(B)$  is seen at  $\sim 1.9$  T which is also the field where the peak at  $N = 22$  would be expected. This feature seems to indicate a change in the viscosity of the liquid, which will be further discussed below. The unexpected increase of  $\rho(B)$  above  $B_{c2}$  until about 3.0 T (not observed in the reference sample) is due to a combination of surface superconductivity at the NbGe channel edges and a proximity effect at the NbN/NbGe interface, as could be proved in recent experiments.

The length scale dependence of the vortex liquid properties is demonstrated in Fig. 2, where a series of  $\rho_{ac}$  data for different channel widths at  $T = 1.70$  K is plotted. Noting that the transition from Ohmic to non-Ohmic behavior occurs at about  $\rho = 0.75 \mu\Omega m$ , we use this criterion to determine the finite size melting field  $B_m(w)$ . Similar results of  $\rho_{ac}(T)$  at  $B = 1.0$  T are shown in the inset. The free dislocations in the liquid near melting will in our configuration line up along the channel edges which allows us to identify  $\xi_+$  with  $w_{eff}$  and check Eq. (2). The results are shown in Fig. 3. The thermodynamic values ( $B_m = 1.54$  T and  $T_m = 2.01$  K) are taken from the data of the reference sample for which  $\xi_+ \approx 300 \mu m$ . The lines represent fits of Eq. (2) providing the values for  $b' = 1.2 \pm 0.1$ ,  $\xi_{+0} = 26 \pm 5$  nm and  $b'' = 1.2 \pm$

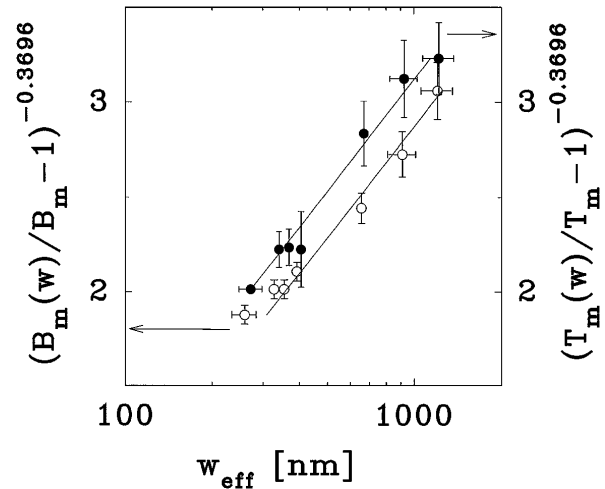


FIG. 3. Finite size effect of the melting temperature  $T_m(w_{eff})$  at  $B = 1.00$  T ( $\bullet$ ) and the melting field  $B_m(w_{eff})$  at  $T = 1.70$  K ( $\circ$ ). Identifying  $\xi_+$  with the effective channel width  $w_{eff}$ , linear fits determine the nonuniversal constants  $b'$ ,  $b''$  and the typical length scale  $\xi_{+0}$  in Eq. (2).

0.1,  $\xi_{+0} = 34 \pm 5$  nm. As should be, the nonuniversal constants are of order 1 and  $\xi_{+0}$  is of order  $b_0$ , the latter being 31–35 nm between 1.5 and 1.9 T and 42 nm at 1.0 T. This confirms quite nicely the predictions of the Nelson-Halperin theory [7]. We should note, however, that similar plots with  $\nu = 0.5$  gave equally reasonable results. So, we cannot discriminate here between a solid-to-hexatic or a hexatic-to-isotropic liquid transition, although the former seems the more likely one, because the channel will promote orientational order. It should further be noted that the criterion  $\rho = 0.75 \mu\Omega m$  is rather arbitrary. In fact, Fig. 2 shows that below this value  $\rho_{ac}$  drops rapidly but not in a sharp step which means that the shear viscosity of the liquid grows quickly, impeding the flow velocity in the channel. The choice of a lower criterion does not change the plots of Fig. 3 qualitatively, but gives slightly different values of the resulting parameters. Similar results are obtained from the experiments at other temperatures and fields.

Finally we can, by using Eq. (4) with  $w_{eff}$ , determine the shear viscosity from the different  $\rho_{ac}$  curves in Fig. 2 plus the  $\rho_f^0$  of the reference sample. The data should result in one curve of  $\eta$  versus  $B$  (or  $T$ ) that follows the functional dependence of  $\xi_+^2/b_0^2$  versus  $B$  (or  $T$ ). This behavior is indeed observed as can be seen in Fig. 4 for  $\eta(B)$  at  $T = 1.70$  K and for  $\eta(T)$  at 1.0 T (inset). The lines display  $\eta = \eta_0 \xi_+^2(B)/b_0^2$  with  $\eta_0 = 2.5 \times 10^{-10} \text{ kg m}^{-1} \text{ s}^{-1}$ . Assuming that we are dealing with a 2D liquid the diffusion constant far in the liquid phase would follow from  $\eta_0 = k_B T / D_0 d$  [11] and we obtain  $D_0 \approx 0.3 \text{ mm}^2/\text{s}$  and a typical diffusion time  $\tau_0 = D_0/a_0^2$  of 2 ns. A remarkable feature is the shoulder in  $\eta(B)$  at 1.9 T. Such a feature is unexpected unless it denotes the transition from a hexatic to isotropic liquid. Below 1.9 T,  $\eta(B)$  would then rather be the effective

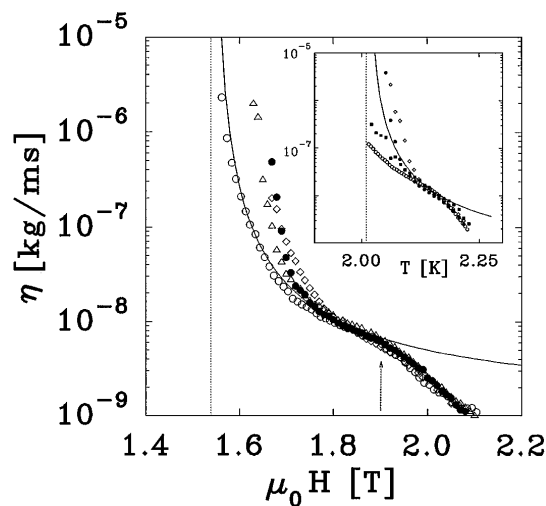


FIG. 4. The shear viscosity  $\eta(B)$  of the flux-line liquid at  $T = 1.70$  K calculated from the resistivity data in Fig. 2 using Eq. (4) for  $w = 1195$  nm ( $\square$ ),  $637$  nm ( $\circ$ ),  $373$  nm ( $\triangle$ ),  $306$  nm ( $\bullet$ ), and  $245$  nm ( $\diamond$ ). The dashed line indicates the thermodynamic melting field  $B_m$ . The curve represents  $\eta = \eta_0 \xi_+^2 / b_0^2$  with  $\eta_0 = 2.5 \times 10^{-10}$  kg m $^{-1}$  s $^{-1}$ . The arrow is the possible location of the hexatic-to-liquid (isotropic) transition. The inset shows  $\eta(T)$  results for the same samples at  $1.00$  T.

viscosity  $\eta_{\text{eff}}$  of the hexatic phase which at the transition reduces to  $\eta$ , the viscosity of the isotropic liquid. Both viscosities are related by  $\eta_{\text{eff}} - \eta \propto K_A$  [8], where the Frank constant  $K_A$  measures the stiffness against bond angle deformations in the hexatic phase. Near the melting line it diverges as  $K_A \sim \xi_+^2$ , i.e., making the behavior of  $\eta_{\text{eff}}$  indistinguishable from that of  $\eta$ . At the hexatic-liquid transition it drops to zero. This second transition is somewhat smeared, but qualitatively agrees with the theoretical prediction [7]. The increase of  $\eta_{\text{eff}}$  at the shoulder agrees reasonably well with the increase by a factor of 2 at the disclination unbinding temperature observed in simulations by Frenkel and McTague [17]. It is remarkable that in our relative thick layers (310 nm) the characteristics of a 2D system are observed. This indicates that the tilt deformations and entanglement of the flux lines play a minor role.

In summary, flow experiments were carried out on flux line solids and liquids confined to narrow channels of various widths  $w$ . Flow-velocity oscillations are observed related to commensurate-incommensurate transitions of the solid with respect to  $w$ . From the period we conclude that the lattice flows along the direction of closed packing and we could determine the effective channel width. An extra peak in the resistivity could be identified as the precursor of the melting transition. The field and temperature of this transition depend on  $w$ . We propose that free dislocations in the liquid line up along the channel edges so that the correlation length  $\xi_+ = w_{\text{eff}}$ .

The temperature and field dependence of  $\xi_+$  agrees well with the Nelson-Halperin theory. The shear viscosity was determined and follows the expectation  $\eta = \eta_0 \xi_+^2 / b_0^2$  with  $\eta_0 = 2.5 \times 10^{-9}$  P. A sudden decrease of  $\eta$  in the liquid may indicate a second transition from hexatic-to-isotropic flux liquid.

We thank K. Pijenburg for experimental assistance and A. Koshelev, V. Vinokur, and D. Nelson for valuable discussions. This work is supported by the Dutch Foundation for Fundamental Research on Matter (FOM).

- [1] G. Eilenberger, Phys. Rev. **164**, 628 (1967).
- [2] D. J. Bishop *et al.*, Bull. Am. Phys. Soc. **33**, 606 (1988); D. R. Nelson, Phys. Rev. Lett. **60**, 1973 (1988).
- [3] H. Safar *et al.*, Phys. Rev. Lett. **69**, 824 (1992); W. K. Kwok *et al.*, Phys. Rev. Lett. **69**, 3370 (1992); W. K. Kwok *et al.*, Phys. Rev. Lett. **72**, 1092 (1994); S. L. Lee *et al.*, Phys. Rev. Lett. **71**, 3862 (1993); R. Cubitt *et al.*, Nature (London) **365**, 407 (1993); E. Zeldov *et al.*, Nature (London) **375**, 373 (1995); H. Pastoriza *et al.*, Phys. Rev. Lett. **75**, 3525 (1995).
- [4] P. Berghuis *et al.*, Phys. Rev. Lett. **65**, 2583 (1990); P. Berghuis *et al.*, Phys. Rev. B **47**, 262 (1993); A. Yazdani *et al.*, Phys. Rev. Lett. **70**, 505 (1993); Y. Volokitin and P. H. Kes, Phys. Rev. B **50**, 13013 (1994).
- [5] A. Zippelius, B. I. Halperin, and D. R. Nelson, Phys. Rev. B **22**, 2514 (1980).
- [6] W. Shockley, in *L'Etat Solide, Proceedings of the Neuvième Conseil de Physique*, edited by R. Stoops (Institut International de Physique Solvay, Brussels, 1952); M. C. Marchetti and D. R. Nelson, Phys. Rev. B **41**, 1910 (1990).
- [7] D. R. Nelson and B. I. Halperin, Phys. Rev. B **19**, 2457 (1979).
- [8] D. R. Nelson, *Phase Transitions and Critical Phenomena*, edited by C. Domb and J. L. Lebowitz (Academic Press, London, 1983), Vol. 7.
- [9] A. Pruijboom, P. H. Kes, E. van der Drift, and S. Radelaar, Phys. Rev. Lett. **60**, 1430 (1988).
- [10] J. Bardeen and M. J. Stephen, Phys. Rev. **140**, A1197 (1965).
- [11] M. C. Marchetti and D. R. Nelson, Phys. Rev. B **42**, 9938 (1990).
- [12] E. van der Drift, S. Radelaar, A. Pruijboom, and P. H. Kes, J. Vac. Sci. Technol. B **6**, 297 (1988).
- [13] F. F. Ternovskii and L. N. Shekhata, Zh. Eksp. Teor. Fiz. **62**, 2297 (1972) [Sov. Phys. JETP **35**, 1202 (1972)]; A. E. Koshelev, Physica (Amsterdam) **223C**, 276 (1994).
- [14] A. E. Koshelev, Phys. Rev. B **50**, 506 (1994); Phys. Rev. B **51**, 12063 (1995).
- [15] G. S. Mkrtchyan, F. R. Shakerzyanova, E. A. Shapoval, and V. V. Shmidt, Zh. Eksp. Teor. Fiz. **63**, 667 (1972) [Sov. Phys. JETP **36**, 352 (1973)].
- [16] S. Bhattacharya and M. J. Higgins, Phys. Rev. Lett. **70**, 2617 (1993); S. Bhattacharya and M. J. Higgins, Phys. Rev. B **49**, 10005 (1994).
- [17] D. Frenkel and J. P. McTague, Phys. Rev. Lett. **42**, 1632 (1979).